Underdetermined DOA estimation of quasi-stationary signals via Khatri–Rao structure for uniform circular array ☆

Ming-Yang Cao [a], Lei Huang [a,*], Cheng Qian [a], Jia-Yin Xue [a], H.C. So [b]

[a] Department of Electronic and Information Engineering, Harbin Institute of Technology, Shenzhen Graduate School, Shenzhen, China
[b] Department of Electronic Engineering, City University of Hong Kong, Hong Kong, China

ARTICLE INFO

ABSTRACT

Underdetermined direction-of-arrival (DOA) estimation for quasi-stationary signals impinging on a uniform circular array (UCA) with M sensors is addressed in this paper. We apply the Khatri–Rao (KR) approach to the UCA and obtain a new signal model which is capable of providing $O(M^2)$ sensors. Meanwhile, the virtual steering matrix can be decomposed into a product of characteristic matrix depending on the array structure and a Vandermonde matrix bearing the DOA information. The exact number of virtual sensors that the KR-UCA model is able to provide is studied as well. Simulation results are included to demonstrate the effectiveness of the proposed method.

© 2014 Elsevier B.V. All rights reserved.

1. Introduction

Quasi-stationary signals (QSS) represent an important class of signals that we frequently encounter in many applications such as microphone array speech processing [1] and electroencephalogram [2]. The QSS has the statistical property that it remains stationary over a short period of time but varies from one time frame to others. This quasi-stationary statistical property in time domain enables us to perform underdetermined direction-of-arrival (DOA) estimation in space domain.

Many methods have been developed to deal with the DOA estimation in the underdetermined condition, such as higher-order cumulants [3] and nested array [4]. Meanwhile, a Khatri–Rao (KR) subspace approach has also been proposed in [5] to tackle the underdetermined DOA estimation of QSSs.

Uniform circular array (UCA) [6] is of interest in many applications, including radar, sonar and navigation, due to its desirable properties. That is, it is capable of providing 360° azimuthal coverage and offers the same aperture for any direction. Basically, there are two main approaches to solve the DOA estimation problem for UCA. The first one is to use the property of Bessel function to fulfil a beamspace transformation [7,8]. The second one is to adopt the concept of virtual array which is developed using the interpolated array (IA) technique [9]. Conventionally, an M-element UCA can resolve up to $(M-1)$ sources. In order to resolve more than $(M-1)$ sources, we might employ the KR subspace approach with UCA to handle the issue of underdetermined DOA estimation and we call this scheme KR-UCA. However, the beamspace transformation technique cannot be applied to the KR-UCA because the

* Corresponding author.
E-mail addresses: cao.myang@gmail.com (M.-Y. Cao),
lhuang8sasp@hotmail.com (L. Huang), alextoqc@gmail.com (C. Qian),
jiayin.xue@gmail.com (J.-Y. Xue), hcso@ee.cityu.edu.hk (H.C. So).

array structure of KR-UCA is different from UCA, and the IA technique introduces mapping errors which in turn considerably degrade the DOA estimation accuracy. Conventional DOA estimation technique, e.g., fourth-order cumulant MUltiple SIgnal Classification (4-MUSIC) [10,11], has a high complexity burden. In this paper, we exploit the manifold separation technique (MST) [12] for KR-UCA DOA estimation. The steering matrix of KR-UCA can be decomposed into the product of a characteristic matrix describing the UCA and a Vandermonde structure containing the DOA information. We then apply the Capon [13] and MUSIC [14] methods to the KR-UCA DOA estimation problem in both narrowband and wideband conditions. Low-complexity methods, e.g., root-MUSIC [15], could also be applied to the KR-UCA. The number of virtual sensors that our proposed method can provide is up to $O(M^2)$. As a result, it can perform underdetermined DOA estimation. In this paper, the UCA sensors have omnidirectional radiation patterns and no mutual coupling effect. Note that a number of methods which can deal with mutual coupling effect for UCA have been proposed in [8,16,17]. It is assumed that each source is located at a fixed and known elevation angle. Hence, we only address 1-D DOA estimation.

This paper is organized as follows. In Section 2, we present the signal model. In Section 3, we review the KR subspace approach and then derive two KR-UCA based DOA estimators using the Capon and MUSIC methods. In Section 4, we include simulation results to illustrate the performance of the algorithms in both narrowband and wideband scenarios. Finally, conclusions are drawn in Section 5.

2. Signal model

Consider a UCA with M uncoupled and omnidirectional sensors. There are P uncorrelated signals impinging on the UCA. The observation vector is

$$\mathbf{x}(t) = \mathbf{A}\mathbf{s}(t) + \mathbf{n}(t), \quad t = 1, \ldots, N. \tag{1}$$

Here, $\mathbf{n}(t) \in \mathbb{C}^M$ is assumed a zero-mean white Gaussian vector with covariance $\sigma_n^2 \mathbf{I}_M$ where $\mathbf{I}_M$ is the $M \times M$ identity matrix, $\mathbf{A} = [\mathbf{a}(\phi_1), \mathbf{a}(\phi_2), \ldots, \mathbf{a}(\phi_P)] \in \mathbb{C}^{M \times P}$ is the steering matrix of UCA and $\mathbf{a}(\phi_p)$ is the $M \times 1$ steering vector:

$$\mathbf{a}(\phi_p) = [e^{j\zeta \cos(\phi_p - \gamma_1)}, e^{j\zeta \cos(\phi_p - \gamma_2)}, \ldots, e^{j\zeta \cos(\phi_p - \gamma_M)}]^T \tag{2}$$

for $p = 1, 2, \ldots, P$. Here, the superscript $(\cdot)^T$ stands for transpose, $j = \sqrt{-1}$, $\gamma_m = 2\pi m/M$, $m = 1, 2, \ldots, M$, $\zeta = \kappa r \sin(\theta)$, r is the radius of the UCA, $\kappa = 2\pi\lambda$ with λ being the wave length, and $\phi_p \in (-\pi, \pi]$ is the azimuth angle. In this paper, we assume that co-elevation angle θ is fixed at $90°$ [9,12]. As a result, $\zeta = 2\pi r/\lambda$ is a constant for fixed elevation angle in the narrowband condition. Moreover, the source number P is *a priori* known or accurately estimated [18–20].

Each source signal $s_p(t)$ is modeled as a quasi-stationary process with K non-overlapped frames and the length of each frame is L. Within the kth frame, the QSS is stationary,

meaning that

$$\mathbb{E}\{|s_p(t)|^2\} = \sigma_{pk}^2, \quad \forall t \in [(k-1)L, \ kL - 1], \ k = 1, 2, \ldots, K \tag{3}$$

where $\mathbb{E}\{\cdot\}$ denotes the expectation operator and signal power σ_{pk}^2 varies along with p and k. The corresponding exact local covariance in the kth frame can be written as

$$\mathbf{R}_k = \mathbb{E}\{\mathbf{x}_k(t)\mathbf{x}_k^H(t)\} = \mathbf{A}\mathbf{D}_k\mathbf{A}^H + \sigma_n^2\mathbf{I}_M \tag{4}$$

where $\mathbf{D}_k = \text{diag}(\sigma_{1k}^2, \sigma_{2k}^2, \ldots, \sigma_{Pk}^2)$, $\mathbf{x}_k(t)$ contains the samples within the kth frame and the superscript $(\cdot)^H$ stands for conjugate transpose.

3. Khatri–Rao subspace approach

In this section, we apply the KR subspace approach to DOA estimation with UCA and derive a new array model of KR-UCA. To begin with, we briefly introduce the property of KR product. We use $\text{vec}(\cdot)$ to represent vectorization, $\odot$ to denote the KR product, $\otimes$ to denote the Kronecker product and the superscript $*$ to denote conjugate. Let $\mathbf{A} \in \mathbb{C}^{M \times P}, \mathbf{D} \in \mathbb{C}^{P \times P}$ and $\mathbf{C} \in \mathbb{C}^{M \times P}$. If $\mathbf{D} = \text{diag}(d_{11}, d_{22}, \ldots, d_{PP})$ is a diagonal matrix, then

$$\text{vec}(\mathbf{A}\mathbf{D}\mathbf{C}^H) = (\mathbf{C}^* \otimes \mathbf{A})\text{vec}(\mathbf{D})$$
$$= (\mathbf{C}^* \odot \mathbf{A})[d_{11}, d_{22}, \ldots, d_{PP}]^T. \tag{5}$$

To exploit the KR subspace, we apply the vectorization in (5) to (4). As a result, we obtain the kth vector $\mathbf{z}_k$:

$$\mathbf{z}_k = \text{vec}(\mathbf{A}\mathbf{D}_k\mathbf{A}^H + \sigma_n^2\mathbf{I}_M)$$
$$= \text{vec}\left(\sum_{p=1}^{P} \sigma_{pk}^2(\mathbf{a}(\phi_p)\mathbf{a}^H(\phi_p))\right) + \text{vec}(\sigma_n^2\mathbf{I})$$
$$= (\mathbf{A}^* \odot \mathbf{A})\mathbf{q}_k + \sigma_n^2\mathbf{1}$$
$$= \mathbf{B}\mathbf{q}_k + \sigma_n^2\mathbf{1} \tag{6}$$

where

$$\mathbf{B} = [\mathbf{b}(\phi_1), \mathbf{b}(\phi_2), \ldots, \mathbf{b}(\phi_P)] \in \mathbb{C}^{M^2 \times P}, \tag{7}$$

$$\mathbf{q}_k = [\sigma_{1k}^2, \sigma_{2k}^2, \ldots, \sigma_{Pk}^2]^T, \tag{8}$$

$$\mathbf{1} = [\mathbf{e}_1^T, \mathbf{e}_2^T, \ldots, \mathbf{e}_P^T]^T. \tag{9}$$

Here, $\mathbf{e}_i$ is a $M \times 1$ vector with one at the ith position and zero otherwise. In (6), the vectorized $\mathbf{R}_k$ behaves like a new signal model. That is, $\mathbf{q}_k$ is the signal vector, $\sigma_n^2\mathbf{1}$ stands for the noise and $\mathbf{B}$ is a steering matrix corresponding to a virtual array which has a larger aperture than that of the array which is not vectorized. Therefore, we can use this property to handle much more signals than the number of sensors in the UCA. Note that this property exists when signals are uncorrelated. For both stationary and quasi-stationary signals, (6) is preserved if the signals are uncorrelated. For the quasi-stationary signals, $\mathbf{q}_k$ varies differently over each frame. So we can apply conventional DOA estimation methods to (6). Also, the noise in (6) behaves like a deterministic vector which could be eliminated easily. In what follows, we refer this signal model to as the KR-UCA.

3.1. Steering matrix of KR-UCA

According to (6) and using the property of Kronecker product, the KR-UCA steering vector $\mathbf{b}(\phi) \in \mathbb{C}^{M^2 \times 1}$ is

$$\mathbf{b}(\phi) = \text{vec}(\mathbf{a}(\phi)\mathbf{a}^H(\phi)) = \mathbf{a}^*(\phi) \otimes \mathbf{a}(\phi)$$

$$= \begin{bmatrix} e^{-j\zeta \cos(\phi-\gamma_1)} \\ e^{-j\zeta \cos(\phi-\gamma_2)} \\ \vdots \\ e^{-j\zeta \cos(\phi-\gamma_M)} \end{bmatrix} \otimes \begin{bmatrix} e^{j\zeta \cos(\phi-\gamma_1)} \\ e^{j\zeta \cos(\phi-\gamma_2)} \\ \vdots \\ e^{j\zeta \cos(\phi-\gamma_M)} \end{bmatrix}$$

$$\triangleq \begin{bmatrix} b_{11} \\ \vdots \\ b_{mn} \\ \vdots \\ b_{MM} \end{bmatrix}, \quad m, n = 1, ..., M$$

$$\triangleq \begin{bmatrix} b_1 \\ \vdots \\ b_i \\ \vdots \\ b_{M^2} \end{bmatrix}, \quad i = 1, ..., M^2. \tag{10}$$

The subscripts m and n in (10) refer to the corresponding element position in $\mathbf{a}^*(\phi)$ and $\mathbf{a}(\phi)$, respectively. The b_{mn} is obtained through the mth element in $\mathbf{a}^*(\theta)$ multiplying by the nth element in $\mathbf{a}(\theta)$. The index i in (10) indicates the element position in $\mathbf{b}(\phi)$. We can give a general expression of $b_{mn}(\phi)$ as

$$b_{mn}(\phi) = e^{j\zeta(\cos(\phi-\gamma_m) - \cos(\phi-\gamma_n))}$$
$$= e^{j(2\pi r/\lambda)(\cos(\phi-\gamma_m) - \cos(\phi-\gamma_n))}$$
$$= e^{j(4\pi r/\lambda) \sin((\gamma_n-\gamma_m)/2) \sin(\phi-(\gamma_n+\gamma_m)/2)}$$
$$= e^{jz_{mn} \sin(\beta_{mn})} \tag{11}$$

where $z_{mn} = (4\pi r/\lambda) \sin((\gamma_n - \gamma_m/2))$, $\beta_{mn} = \phi - (\gamma_n + \gamma_m/2)$ and $\eta_{mn} = (\gamma_n + \gamma_m/2)$. Using the Jacobi–Anger expansion in [21], we have

$$b_{mn}(\phi) = e^{jz_{mn} \sin(\beta_{mn})} = \sum_{h=-\infty}^{\infty} J_h(z_{mn})e^{jh\beta_{mn}}$$
$$= \sum_{h=-\infty}^{\infty} J_h(z_{mn})e^{-jh\eta_{mn}}e^{jh\phi} \tag{12}$$

where $J_h(z)$ stands for Bessel function of the first kind of mode h. The steering vector $\mathbf{b}(\phi)$ could thereby be modeled as

$$b_{mn} = \mathbf{p}_{mn}^T \mathbf{d}(\phi) \tag{13}$$

where $\mathbf{p}_{mn}$ and Vandermonde vector $\mathbf{d}(\phi)$ have the following expressions:

$$\mathbf{p}_{mn} = [..., J_{-2}(z_{mn})e^{j2\eta_{mn}}, \ J_{-1}(z_{mn})e^{j\eta_{mn}},$$
$$J_0(z), J_1(z_{mn})e^{-j\eta_{mn}}, J_2(z_{mn})e^{-j2\eta_{mn}}, ...]^T, \tag{14}$$

$$\mathbf{d}(\phi) = [..., e^{-j2\phi}, \ e^{-j\phi}, 1, e^{j\phi}, e^{j2\phi}, ...]^T. \tag{15}$$

Substituting (13) into (10) yields

$$\mathbf{b}(\phi) = [b_{11}, b_{12}, ..., b_{MM}]^T$$
$$= [\mathbf{p}_{11}^T \mathbf{d}(\phi), \mathbf{p}_{12}^T \mathbf{d}(\phi), ..., \mathbf{p}_{MM}^T \mathbf{d}(\phi)]^T$$
$$= \mathbf{Pd}(\phi) \tag{16}$$

where

$$\mathbf{P} = [\mathbf{p}_{11}, \mathbf{p}_{12}, ..., \mathbf{p}_{MM}]^T. \tag{17}$$

Note that $\mathbf{P}$ is the characteristic matrix of the KR-UCA, which depends only on the array configuration.

According to (16), the steering matrix of the KR-UCA can be written as

$$\mathbf{B} = \mathbf{PD}. \tag{18}$$

where

$$\mathbf{D} = [\mathbf{d}(\phi_1), \mathbf{d}(\phi_2), ..., \mathbf{d}(\phi_P)]. \tag{19}$$

Based on (18), we accurately express the steering matrix $\mathbf{B}$ by using infinite number of modes in $\mathbf{d}(\phi)$ and $\mathbf{p}$.

Thus, we could use finite H_e modes to approximate $\mathbf{B}$, and rewrite (12) as

$$b_{mn} = \sum_{h=-(H_e-1)/2}^{(H_e-1)/2} J_h(z_{mn})e^{-jh\eta_{mn}}e^{jh\phi} + \epsilon(H_e) \tag{20}$$

where the truncated error $\epsilon(H_e)$ is a function of mode number H_e. As discussed in [22], the magnitude of Bessel function in (15) decays super-exponentially with increasing H_e. It means that as $H_e \rightarrow \infty$, the truncated error $\epsilon(H_e) \rightarrow 0$. Therefore, a finite number of H_e modes achieves high accuracy, enabling us to use a truncated $\mathbf{p}_{mn}$ to approximate the original one in (16), that is,

$$b_{mn} \approx \sum_{h=-(H_e-1)/2}^{(H_e-1)/2} J_h(z_{mn})e^{-jh\eta_{mn}}e^{jh\phi}. \tag{21}$$

Note that selection of H_e has been discussed in [22]. A rule-of-thumb of H_e is given as $H_e = 4\kappa R$, and R is the largest distance between a virtual sensor and the center of the UCA which is given in (2). According to (11), the distance between an array sensor and the center of the UCA is $2r \sin((\gamma_n - \gamma_m)/2)$. So the maximum of the distances could reach is $2r$. Therefore, H_e of KR-UCA is chosen as

$$H_e = 8\kappa r. \tag{22}$$

We define the normalized truncation error as

$$\epsilon_{err}(H_e) = \frac{\|\mathbf{Pd}(\phi) - \mathbf{b}(\phi)\|_F}{\|\mathbf{b}(\phi)\|_F}. \tag{23}$$

We set $M=5$ and give a numerical example in Table 1.

Table 1 shows that $\epsilon_{err}(H_e)$ decreases as H_e increases and increases as r increases. The $\epsilon_{err}(H_e)$ is negligible when H_e is sufficiently large, e.g., $H_e = 71$. Therefore, the steering vector of KR-UCA is expressed as a product of characteristic matrix and a Vandermonde matrix bearing DOA information with negligible transformation error. This property enables us to employ the low-complexity algorithms, such as root-MUSIC for DOA estimation.

For an M-element KR-UCA, the number of virtual sensors is M^2. However, some of the virtual sensors may

Table 1
Normalized truncation error as a function of UCA radius and mode number H_e.

$r(\lambda)$	$H_e=11$	$H_e=31$	$H_e=71$
0.6	5.7×10^{-1}	2.8×10^{-5}	1.2×10^{-14}
1.6	7.2×10^{-1}	4.3×10^{-1}	4.1×10^{-8}

coincide and this thereby reduces the array aperture. The relationship between the number of different virtual sensors r in **B** and M is given by the following proposition.

Proposition 1. *Given M elements of a KR-UCA, the maximum number of different virtual sensors is*

$$l = \begin{cases} M^2/2 + 1 & \text{if } M \text{ is even} \\ M^2 - M + 1 & \text{if } M \text{ is odd}. \end{cases} \tag{24}$$

The proof is given in Appendix A.

Note that the structure of steering matrix of KR-UCA is similar to that of the fourth-order cumulants and the different virtual sensors have been discussed in [3,23].

3.2. KR-UCA DOA estimation for narrowband signals

Recall (6), the noise behaves like a deterministic vector. It only has σ_n^2 at $((M+1)i+1)$th positions, $i = 0, 1, ..., M-1$, the others are zeros. Observing that, we delete the $(M+1)i+1$th rows of $\mathbf{z}_k$, $i = 0, 1, ..., M-1$, to eliminate noise. After deletion, the remaining part is

$$\overline{\mathbf{z}}_k = \overline{\mathbf{B}}\mathbf{q}_k = \overline{\mathbf{P}}\mathbf{D}\mathbf{q}_k \tag{25}$$

where

$$\overline{\mathbf{P}} = [\mathbf{p}_{12}, \mathbf{p}_{13}, ..., \mathbf{p}_{21}, \mathbf{p}_{23}, ..., \mathbf{p}_{M(M-1)}]^T. \tag{26}$$

Thus (25) becomes a noise free signal model after deletion and it is convenient to apply MUSIC algorithm to it. Note that the number of virtual sensors of $\overline{\mathbf{z}}_k$ only decreases one. We stack $\overline{\mathbf{z}}_k$, $k = 1, ..., K$, into a matrix to yield

$$\overline{\mathbf{Z}} = [\overline{\mathbf{z}}_1, \overline{\mathbf{z}}_2, ..., \overline{\mathbf{z}}_K] = \overline{\mathbf{P}}\mathbf{D}\Xi \tag{27}$$

where

$$\Xi = [\mathbf{q}_1, \mathbf{q}_2, ..., \mathbf{q}_K]. \tag{28}$$

For a finite number of K, the exact covariance matrix $\mathbf{R}_Q$ could not be obtained. The corresponding sample covariance matrix is calculated as

$$\hat{\mathbf{R}}_Q = \frac{1}{K}\overline{\mathbf{Z}}\overline{\mathbf{Z}}^H. \tag{29}$$

Notice that the source signal vector $\mathbf{q}_k$ is different over time frames due to the property of QSS. As a result, the source power matrix Ξ has full column rank, indicating that

$$\text{rank}(\overline{\mathbf{Z}}) = \text{rank}(\overline{\mathbf{P}}\mathbf{D}). \tag{30}$$

By performing the singular value decomposition (SVD) on $\hat{\mathbf{R}}_Q$, we get the estimated noise subspace $\hat{\mathbf{U}}_n$. Thus, the KR-UCA MUSIC function is

$$S_{\text{KR–MUSIC}}(\phi) = \frac{1}{\mathbf{d}^H(\phi)\overline{\mathbf{P}}^H\hat{\mathbf{U}}_n\hat{\mathbf{U}}_n^H\overline{\mathbf{P}}\mathbf{d}(\phi)}. \tag{31}$$

The DOAs can be estimated by performing 1-D peak search of $S_{\text{KR–MUSIC}}(\phi)$ in the range of $\phi \in (-\pi, \pi]$. The identifiability condition has to satisfy

$$\mathbf{d}(\phi_{q_1}) \neq \mathbf{d}(\phi_{q_2}) \tag{32}$$

for $\phi_{q_1} \neq \phi_{q_2}$ and $\phi \in (-\pi, \pi]$.

The KR-UCA based DOA estimation can also be achieved through the Capon method. Applying the Capon method to

the KR-UCA, the Capon based KR-UCA DOA estimator is to find the P peaks of

$$S_{\text{KR–Capon}}(\phi) = \frac{1}{\overline{\mathbf{b}}(\phi)^H\hat{\mathbf{R}}_Q^{-1}\overline{\mathbf{b}}(\phi)}. \tag{33}$$

3.3. Extension to wideband signals

For wideband signals with a bandwidth B, we perform the short-time Fourier transform (STFT) to the received data in (1), leading to

$$\tilde{\mathbf{X}}(f, t) \approx \mathbf{A}(f)\tilde{\mathbf{S}}(f, t) + \tilde{\mathbf{N}}(f, t) \tag{34}$$

where $\mathbf{A}(f) = [\mathbf{a}(f, \phi_1), \mathbf{a}(f, \phi_2), ..., \mathbf{a}(f, \phi_P)]$, $\mathbf{a}(f, \phi)$ is the steering vector of UCA in wideband condition, given as

$$\mathbf{a}(f, \phi) = [e^{j\zeta\Delta f \cos(\phi_p - \gamma_1)}, e^{j\zeta\Delta f \cos(\phi_p - \gamma_2)}, ..., e^{j\zeta\Delta f \cos(\phi_p - \gamma_M)}]^T. \tag{35}$$

Here, the frequency $f \in \left[-\frac{1}{2}, \frac{1}{2}\right]$ stands for the normalized frequency, $\Delta = d/(cT_s)$, d is the successive sensor displacement and T_s is the sampling period. The $\tilde{\mathbf{S}}(f, t) \in \mathbb{C}^{M \times N}$ and $\tilde{\mathbf{N}}(f, t) \in \mathbb{C}^{M \times N}$ are defined as the STFTs of $\mathbf{S}(t)$ and $\mathbf{N}(t)$, respectively, within each frequency bin, $\tilde{s}(f, t)$ is a sample in time domain of a fixed frequency bin. Consequently, the STFT of $x(t)$ with a window length of N_{STFT} is defined as

$$\tilde{x}(f, t) = \sum_{u=0}^{N_{\text{STFT}}-1} x(t+u)e^{-j2\pi ft}. \tag{36}$$

The STFTs of $s(t)$ and $n(t)$ are defined as the same way as $x(t)$ in (36). Notice that, for each fixed frequency bin, the received data can be regarded as narrowband condition. The KR-UCA scheme is applied to $\tilde{\mathbf{x}}(f, t)$ of all frequency bins. Then we combine all wideband KR-UCA spectra for final estimation. The wideband KR-UCA MUSIC (WB-KR-MUSIC) spectrum within $B = \{f = i/N_{\text{STFT}} | i = 0, ..., N_{\text{STFT}} - 1\}$ denoted by $S_{\text{WB–KR–MUSIC}}(\phi)$ is given as

$$S_{\text{WB–KR–MUSIC}}(\phi) = \frac{1}{\sum_{i=0}^{N_{\text{STFT}}-1}\|\hat{\mathbf{U}}_n^H(f_i)\overline{\mathbf{P}}(f_i)\mathbf{d}(\phi)\|^2}. \tag{37}$$

It should be noticed that $\mathbf{d}(\phi)$ is independent of frequency. For each frequency bin, the characteristic matrix $\overline{\mathbf{P}}(f_i)$ and the noise subspace $\hat{\mathbf{U}}_n(f_i)$ should be recalculated. We calculate $\hat{\mathbf{R}}_Q(f)$ by (29) for each frequency bin in B. The wideband KR-UCA Capon (WB-KR-Capon) spectrum, denoted by $S_{\text{WB–KR–Capon}}(\phi)$, is

$$S_{\text{WB–KR–Capon}}(\phi) = \frac{1}{\sum_{i=0}^{N_{\text{STFT}}-1}\mathbf{b}_{f_i}^H(\phi)\hat{\mathbf{R}}_Q^{-1}(f_i)\mathbf{b}_{f_i}(\phi)}. \tag{38}$$

4. Simulation results

We provide simulation results for different settings to evaluate the performances of the KR-UCA approach for DOA estimation in this section.

4.1. Narrowband KR-UCA DOA estimation

In this subsection, we use the QSS which obeys Laplacian distribution corrupted by the white Gaussian noise. The

frame length is $L=400$ and the frame number is $K=30$. The radius of the UCA is $r=0.4\lambda$, $M=5$ and the signal-to-noise ration (SNR) is 5 dB. According to (22), we have $H_e>20$. So it is appropriate to choose $H_e=45$ as the mode number.

First, we consider both overdetermined and underdetermined DOA estimation conditions to compare the performances of the estimators in (31) and (33) and 4-MUSIC [10,11]. Figs. 1 and 2 plot ten typical independent estimated spatial spectra of the KR-MUSIC, KR-Capon and 4-MUSIC methods where the dashed lines denote the true DOAs. It is seen that even when the number of signals is larger than the number of sensors, both the KR-UCA

MUSIC and Capon methods could correctly estimate the DOAs. Note that both of the MUSIC and Capon techniques have very sharp spectral peaks and the MUSIC generates less grating lobes than the Capon method. On the other hand, 4-MUSIC method performs poorly in the underdetermined condition.

4.2. Wideband KR-UCA DOA estimation

In the wideband DOA situation, we adopt wideband QSS as the source signal. The frame number is $K=30$, the frame length is $L=400$, the sampling frequency is 8 kHz,
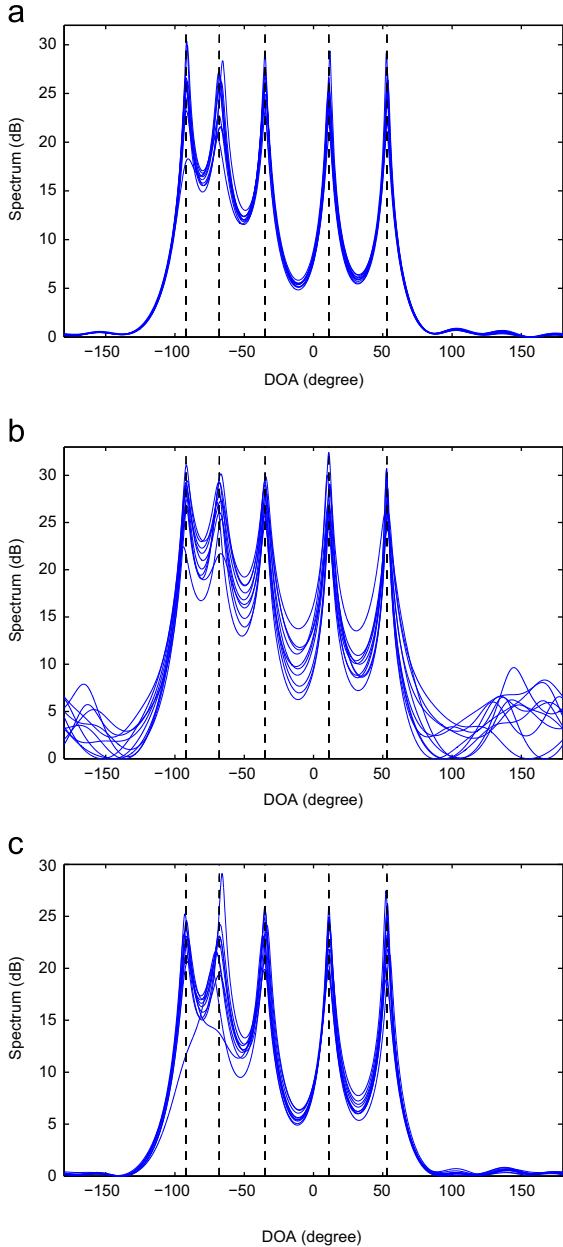

Fig. 1. Narrowband DOA spectra of KR-MUSIC (a), KR-Capon (b) and 4-MUSIC (c), $M=5$, $L=400$, $K=30$, SNR$=5$ dB, DOAs$=\{-92°, -68°, -35°, 11°, 53°\}$.

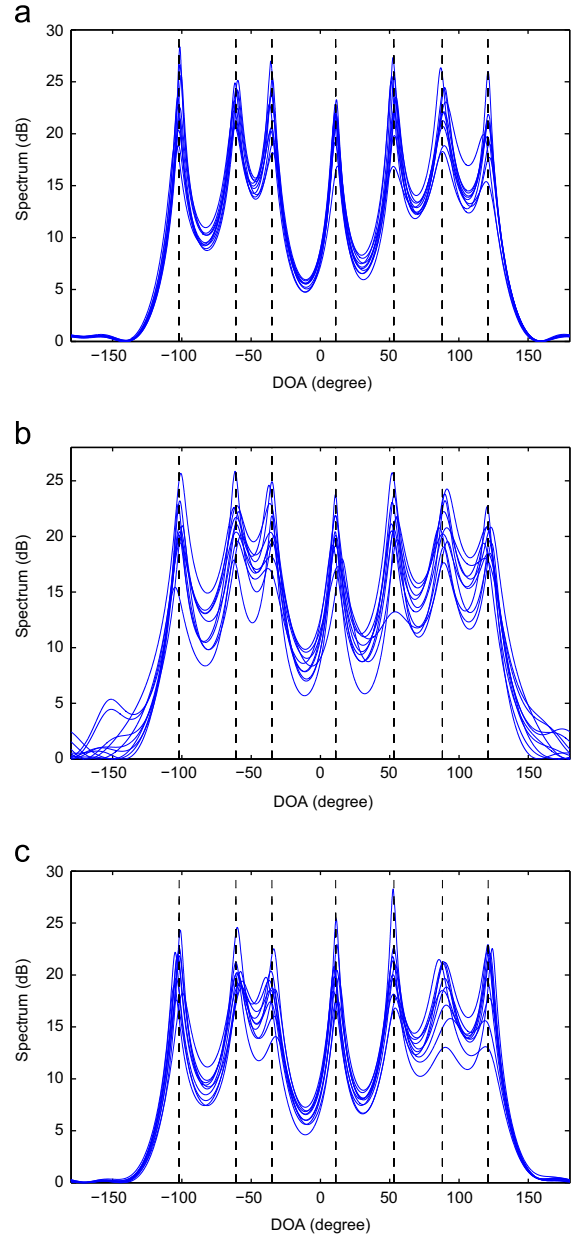**Fig. 2.** Narrowband DOA estimation spectra of KR-MUSIC (a), KR-Capon (b) and 4-MUSIC (c), $M=5$, $r=0.4\lambda$, $L=400$, $K=30$, DOAs$=\{-102°, -61°, -35°, 11°, 53°, 88°, 121°\}$.

$r = 1.0\lambda$, $M = 5$, SNR $= 10$ dB, the signal propagation speed equals 340 m / s, the window length of N_{STFT} is 32 and the normalized frequency is $[1:N_{STFT}-1]/2N_{STFT}$. We use all normalized frequency bins to estimate the DOAs by (37). As displayed in Fig. 3, the KR-UCA based wideband MUSIC and Capon methods could accurately estimate DOAs in both overdetermined and underdetermined cases. However, in the underdetermined condition, the 4-MUSIC method could not correctly estimate the DOAs and we observe that two peaks have merged into one. The KR-MUSIC and KR-Capon methods show a better DOA estimation performance over 4-MUSIC method.

4.3. RMSE performance

In this subsection, we compare the root mean squared errors (RMSEs) and CPU times of KR-UCA Capon, MUSIC, root-MUSIC and 4-MUSIC methods. The independent trial number is 500. The RMSE is defined as

$$\text{RMSE} = \sqrt{\mathbb{E}\left\{\frac{1}{P}\sum_{p=1}^{P}(\hat{\theta}_p - \theta_p)^2\right\}} \qquad (39)$$

where $\hat{\theta}_p$ and θ_p denote the estimated and true DOA, respectively. In all simulations, we set $P = 5$ and $H_e = 45$.

In Figs. 4–6, we compare KR-UCA Capon, MUSIC, root-MUSIC and 4-MUSIC methods by plotting the RMSE performance versus both SNR and radius, CPU time versus the number of array sensors (on a PC equipped with a 2.6 GHz processor, 4 GB of RAM and Matlab R2012a version). We set $L = 400$ and $K = 30$. Fig. 4 shows the RMSE performance of these methods versus SNR with $M = 5$ and

Fig. 4. Comparison of RMSE angle performance versus SNR of KR-MUSIC, KR-root-MUSIC, KR-Capon and 4-MUSIC algorithms, $M = 5$, $P = 5$, $r = 0.5\lambda$, $L = 400$, $K = 30$.

Fig. 5. Comparison of CPU time versus the number of array sensors of KR-MUSIC, KR-root-MUSIC, KR-Capon and 4-MUSIC algorithms, $P = 5$, $L = 400$, $K = 30$, SNR $= 5$ dB $M = 5$, with $r = 0.4\lambda$, $M = 7$ with $r = 0.6\lambda$.
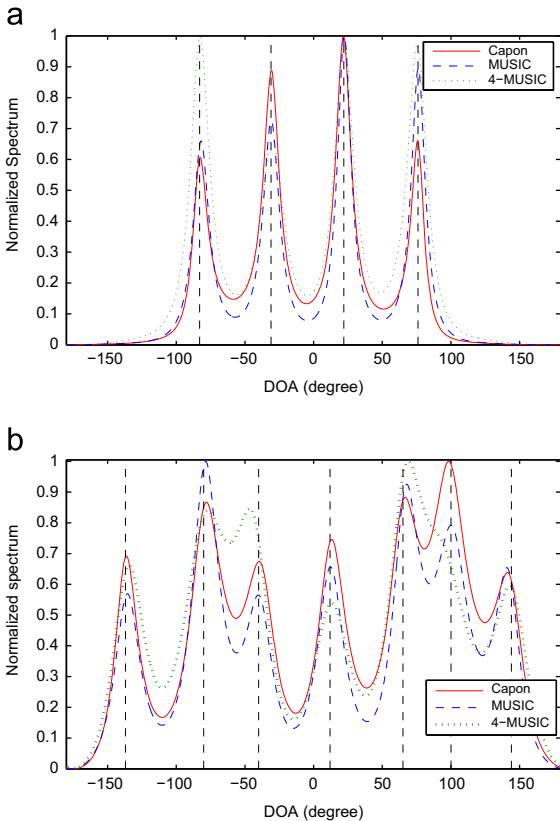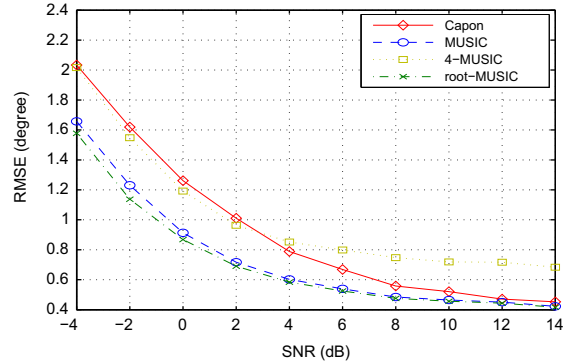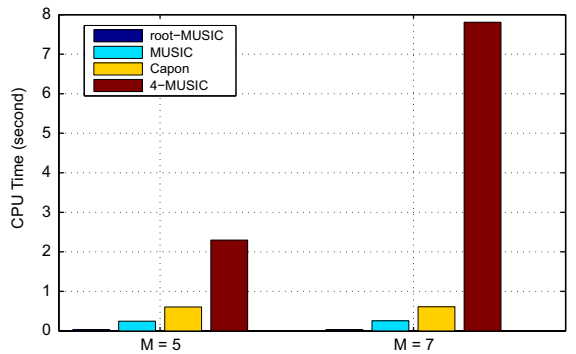

Fig. 3. Wideband DOA estimation spectra of KR-MUSIC, KR-Capon and 4-MUSIC, $M = 5$, $r = 1.0\lambda$, $L = 400$, $K = 30$, SNR $= 10$ dB. (a) DOAs $= \{-83°, -31°, 22°, 76°\}$. (b) DOAs $= \{-137°, -93°, -41°, 12°, 66°, 132°\}$.
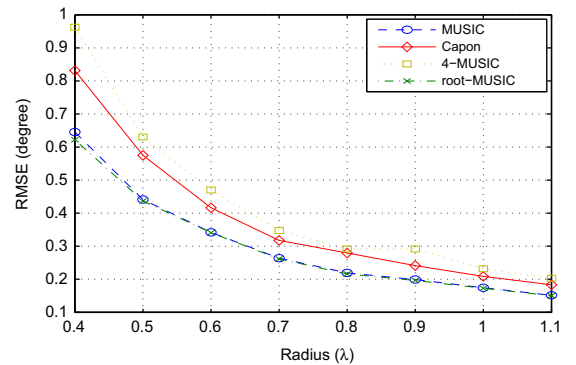

Fig. 6. Comparison of RMSE angle performance versus UCA radius of KR-MUSIC, KR-root-MUSIC, KR-Capon and 4-MUSIC algorithms, $M = 5$, $P = 5$, $L = 400$, $K = 30$, SNR $= 5$ dB.
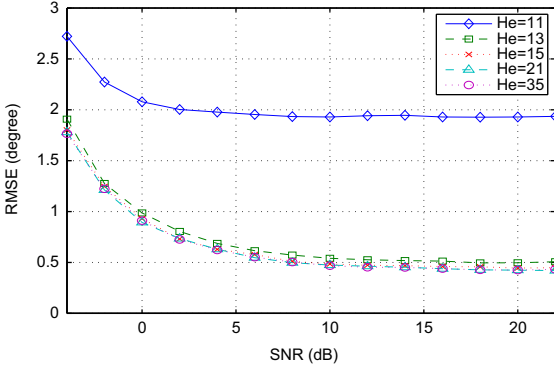
Fig. 7. Comparison of RMSE performance versus SNR of KR-MUSIC with different number of modes, $M=5, P=5, N=12,000$, SNR$=5$ dB.
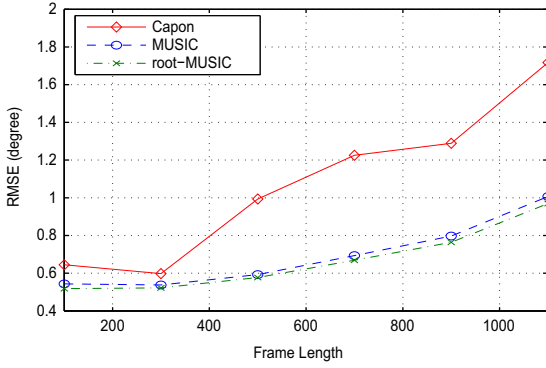

Fig. 8. Comparison of RMSE performance versus frame length of KR-MUSIC, KR-root-MUSIC and KR-Capon algorithms, $M=5, P=5, N=12,000$, SNR$=5$ dB.

$r=0.4\lambda$. It can be seen that KR-UCA root-MUSIC method offers the lowest RMSE. At high SNRs, t.he RMSEs of root-MUSIC, MUSIC, Capon are almost the same, and 4-MUSIC method has the worst accuracy for QSSs. Fig. 5 shows their average CPU times at SNR$=5$ dB. We set $M=5$ and $r=0.4\lambda$; $M=7$ and $r=0.6\lambda$. Note that the CPU times of KR-UCA MUSIC, Capon and 4-MUSIC methods are highly related with the search grid of θ. In this simulation, we set the grid size as $0.01°$. Fig. 6 shows the impact of array radius with $M=5$.

Fig. 7 shows the impact of H_e on the RMSE performance of KR-UCA root-MUSIC method. We set the radius of the UCA as 0.4λ. If we set $H_e=11$, the performance of KR-UCA MUSIC method degrades. When $H_e \geq 15$, the performance of MUSIC method is almost the same. In Fig. 8, we plot the RMSE performance versus L for the KR-UCA root-MUSIC, MUSIC and Capon methods where $K \times L$ is fixed. We see that the RMSE performance degrades when L is large.

5. Conclusion

In this paper, we have proposed the KR-UCA scheme for underdetermined DOA estimation of the QSSs. We have discussed the number of virtual sensors of the KR-UCA. The numbers of virtual sensors for odd and even M are M^2-M+1 and $M^2/2+1$, respectively. Therefore, the KR-UCA is able to achieve underdetermined DOA estimation.

We have investigated the relationship of the RMSE performance with the array radius, number of modes and length of a frame with a fixed number of samples. Moreover, we have extended the KR-UCA estimation to the wideband QSS scenarios. Simulations results are in line with the theoretical analysis.

Appendix A. Proof of Proposition 1

Let us consider a KR-UCA with M physical sensors. The $\mathbf{b}(\phi)$ denotes the steering vector of KR-UCA as defined in (10). The number of actually realizable virtual sensors is determined by the distinct elements in $\mathbf{b}(\phi)$. The repeated elements in $\mathbf{b}(\phi)$ satisfy

$$b_{i_1}(\phi) = b_{i_2}(\phi), \quad i_1 \neq i_2 \tag{A.1}$$

where $b_{i_1}(\phi)$ and $b_{i_2}(\phi)$ stand for the i_1th and i_2th elements of $b_i(\phi)$, respectively, $1 \leq i_1, i_2 \leq M^2$. Recall (12), the coefficients of the hth modes of $b_{i_1}(\phi)$ and $b_{i_2}(\phi)$ are calculated as

$$\frac{1}{2\pi}\int_0^{2\pi} b_{i_1}(\phi)e^{jh\phi}\,d\phi = J_h(z_{i_1})e^{-jh\eta_{i_1}}, \tag{A.2}$$

$$\frac{1}{2\pi}\int_0^{2\pi} b_{i_2}(\phi)e^{jh\phi}\,d\phi = J_h(z_{i_2})e^{-jh\eta_{i_2}}. \tag{A.3}$$

Substituting (A.1) (into A.2) and (A.3), we obtain the equivalent expression of (A.1) as

$$J_h(z_{i_1})e^{-jh\eta_{i_1}} = J_h(z_{i_2})e^{-jh\eta_{i_2}}, \quad i_1 \neq i_2, \tag{A.4}$$

where $h = -\infty, ..., \infty$. Since $J_h(z) \in \mathbb{R}$, $e^{-jh(\eta_{i_1}-\eta_{i_2})} = J_h(z_{i_2})/J_h(z_{i_1})$ is real with modules of 1. According to the value of z, we have two cases:

• *Case* 1: $z \neq 0$. We get two possible situations

$$J_h(z_{i_1}) = J_h(z_{i_2}), \tag{A.5}$$

$$J_h(z_{i_1}) = -J_h(z_{i_2}). \tag{A.6}$$

Let us first consider $J_h(z_{i_1}) = J_h(z_{i_2})$, $e^{-jh\eta_{i_1}} = e^{-jh\eta_{i_2}}$, we have $z_{i_1} = z_{i_1}$ and $\eta_{i_1} = \eta_{i_2}$ by utilizing the characteristics of Bessel function and exponential function, respectively. According to definitions of z and η in (11), we have

$$\begin{cases} \sin\left(\dfrac{\gamma_{n_{i_1}}-\gamma_{m_{i_1}}}{2}\right) = \sin\left(\dfrac{\gamma_{n_{i_2}}-\gamma_{m_{i_2}}}{2}\right) \\ \dfrac{\gamma_{m_{i_1}}+\gamma_{n_{i_1}}}{2} = \dfrac{\gamma_{m_{i_2}}+\gamma_{n_{i_2}}}{2} \end{cases}. \tag{A.7}$$

If $\sin((\gamma_{n_{i_1}}-\gamma_{m_{i_1}})/2) = \sin((\gamma_{n_{i_2}}-\gamma_{m_{i_2}})/2)$, we obtain $(\gamma_{n_{i_1}}-\gamma_{m_{i_1}})/2 = (\gamma_{n_{i_2}}-\gamma_{m_{i_2}})/2$ or $((\gamma_{n_{i_1}}-\gamma_{m_{i_1}})/2)+((\gamma_{n_{i_2}}-\gamma_{m_{i_2}})/2) = \pi$. Recall that $\gamma_m = 2\pi m/M$, the two conditions of (A.7) are expressed as

$$\begin{cases} n_{i_1}-m_{i_1} = n_{i_2}-m_{i_2} \\ n_{i_1}+m_{i_1} = n_{i_2}+m_{i_2} \end{cases} \tag{A.8}$$

or

$$\begin{cases} \dfrac{n_{i_1}-m_{i_1}}{2}+\dfrac{n_{i_2}-m_{i_2}}{2} = \dfrac{M}{2} \\ n_{i_1}+m_{i_1} = n_{i_2}+m_{i_2}. \end{cases} \tag{A.9}$$

The solution of (A.8) is $i_1 = i_2$ and it is contradicted to our assumption.

Simplifying (A.9), we obtain

$$\begin{cases} n_{i_1} = \dfrac{M}{2} + m_{i_2}, & 1 \le n_{i_1}, \ m_{i_2} \le M \quad \text{(A.10a)} \\ n_{i_2} = \dfrac{M}{2} + m_{i_1}, & 1 \le n_{i_2}, \ m_{i_1} \le M \quad \text{(A.10b)} \end{cases}$$

The solutions of (A.10a) are listed as $\{n_{i_1}, m_{i_2}\} = \{1, (M/2)+1\}, \ldots, \{M/2, M\}$ and the solutions of (A.10b) are $\{n_{i_2}, m_{i_1}\} = \{1, (M/2)+1\}, \ldots, \{M/2, M\}$. Thus the number of combinations of these solutions is $M/2 \times M/2 = M^2/4$. However considering that $i_1 \ne i_2$, n_{i_1} and m_{i_1} must have $n_{i_1} - m_{i_2} \ne M/2$, there are $M/2$ solutions that do not satisfy (44). As a result, the number of solutions is

$$\frac{M}{2} \times \frac{M}{2} - \frac{M}{2} = \frac{M^2}{4} - \frac{M}{2}. \tag{A.11}$$

Let us now consider $J_h(z_{i_1}) = -J_h(z_{i_2})$, $e^{-jh\eta_{i_1}} = -e^{-jh\eta_{i_2}}$ for odd mode h and $J_h(z_{i_1}) = J_h(z_{i_2})$, $e^{-jh\eta_{i_1}} = e^{-jh\eta_{i_2}}$ for even mode h. For Bessel function, we have $J_h(-z) = (-1)^h J_h(z)$, thereby the relationships of z_{i_1}, z_{i_2} and η_{i_1}, η_{i_2} of (A.6) are $z_{i_1} = -z_{i_2}$ and $\eta_{i_1} - \eta_{i_2} = \pi$, respectively. The (A.6) is simplified as

$$\begin{cases} n_{i_1} - m_{i_1} = -(n_{i_2} - m_{i_2}) \\ \dfrac{n_{i_1} + m_{i_1}}{2} - \dfrac{n_{i_2} + m_{i_2}}{2} = \dfrac{M}{2}. \end{cases} \tag{A.12}$$

Reorganizing (A.12), we obtain

$$\begin{cases} m_{i_1} = \dfrac{M}{2} + n_{i_2}, & 1 \le n_{i_2}, \ m_{i_1} \le M \quad \text{(A.13a)} \\ n_{i_1} = \dfrac{M}{2} + m_{i_2}, & 1 \le n_{i_1}, \ m_{i_2} \le M. \quad \text{(A.13b)} \end{cases}$$

The solutions of (A.13a) are listed as $\{n_{i_2}, m_{i_1}\} = \{1, (M/2)+1\}, \ldots, \{M/2, M\}$ and the solutions of (A.13b) are listed as $\{m_{i_2}, n_{i_1}\} = \{1, M/2+1\}, \ldots, \{M/2, M\}$. The number of combinations of solutions in (A.13a) and (A.13b) is $M/2 \times M/2 = M^2/4$. However solutions that satisfy $n_{i_1} = m_{i_1}$ and $n_{i_2} = m_{i_2}$ in (A.12) lead to $z=0$. It is contradicted to our assumption. The number of these conditions is $M/2$. As a result, the number of same elements is

$$\frac{M}{2} \times \frac{M}{2} - \frac{M}{2} = \frac{M^2}{4} - \frac{M}{2}. \tag{A.14}$$

- *Case* 2: $z=0$. In this case, we have $m=n$, thus the number of same elements is $M-1$.

Note that the existence of the above-mentioned cases depends on the parity of M. It is clear to see that if M is even, the total number of virtual sensors is

$$M^2 - \left(\frac{M^2}{4} - \frac{M}{2}\right) - \left(\frac{M^2}{4} - \frac{M}{2}\right) - (M-1) = \frac{M^2}{2} + 1. \tag{A.15}$$

If M is odd, then Case 1 does not exist because $M/2$ is no longer an integer in (A.9) and (A.12). Thus, the total number of virtual sensors is

$$M^2 - (M-1) = M^2 - M + 1. \tag{A.16}$$

This completes the proof of Proposition 1.

References

[1] F. Asano, S. Hayamizu, T. Yamada, S. Nakamura, Speech enhancement based on subspace method, IEEE Trans. Speech Audio Process. 8 (September (5)) (2000) 497–507.

[2] L. Rankine, N. Stevenson, M. Mesbah, B. Boashash, A nonstationary model of newborn EEG, IEEE Trans. Biomed. Eng. 54 (January (1)) (2007) 19–28.

[3] P. Chevalier, L. Albera, A. Ferreol, P. Comon, On the virtual array concept for higher order array processing, IEEE Trans. Signal Process. 53 (April (4)) (2005) 1254–1271.

[4] P. Pal, P.P. Vaidyanathan, Nested arrays: a novel approach to array processing with enhanced degrees of freedom, IEEE Trans. Signal Process. 58 (August (8)) (2010) 4167–4181.

[5] W.-K. Ma, T.-H. Hsieh, C.-Y. Chi, Underdetermined DOA estimation of quasi-stationary signals with unknown spatial noise covariance: a Khatri–Rao subspace approach, IEEE Trans. Signal Process. 58 (April (4)) (2010) 2168–2180.

[6] H.L. Van Trees, Detection, Estimation, and Modulation Theory. Part IV. Optimum Array Processing, Wiley, New York, 2002.

[7] C.P. Mathews, M.D. Zoltowski, Eigenstructure techniques for 2-D angle estimation with uniform circular arrays, IEEE Trans. Signal Process. 42 (September (9)) (1994) 2395–2407.

[8] R. Goossens, H. Rogier, S. Werbrouck, UCA root-MUSIC with sparse uniform circular arrays, IEEE Trans. Antennas Propag. 56 (August (8)) (2008) 4095–4099.

[9] B. Friedlander, The root-MUSIC algorithm for direction finding with interpolated arrays, Signal Process. 30 (1993) 15–29.

[10] B. Porat, B. Friedlander, Direction finding algorithms based on high-order statistics, IEEE Trans. Signal Process. 39 (September (9)) (1991) 2016–2024.

[11] S. Shamsunder, G.B. Giannakis, Modeling of non-Gaussian array data using cumulants: DOA estimation of more sources with less sensors, Signal Process. 30 (1993) 279–297.

[12] F. Belloni, A. Richter, V. Koivunen, DOA estimation via manifold separation for arbitrary array structures, IEEE Trans. Signal Process. 55 (October (10)) (2007) 4800–4810.

[13] J. Capon, High-resolution frequency-wavenumber spectrum analysis, Proc. IEEE 57 (8) (1969) 1408–1418.

[14] R. Schmidt, Multiple emitter location and signal parameter estimation, IEEE Trans. Antennas Propag. 34 (March) (1986) 276–280.

[15] A.J. Barabell. Improving the resolution performance of eigenstructure-based direction-finding algorithms, In: Proceedings of the ICASSP'83, Boston, MA, 1983, pp. 336–339.

[16] B.H. Wang, H.T. Hui, M.S. Leong, Decoupled 2D direction of arrival estimation using compact uniform circular arrays in the presence of elevation-dependent mutual coupling, IEEE Trans. Antennas Propag. 58 (March (3)) (2010) 747–755.

[17] J. Xie, Z. He, H. Li, J. Li, 2D DOA estimation with sparse uniform circular arrays in the presence of mutual coupling, EURASIP J. Adv. Signal Process. 2011 (2011) 127.

[18] M. Wax, T. Kailath, Detection of signals by information theoretic criteria, IEEE Trans. Acoust., Speech, Signal Process. 33 (April (2)) (1985) 387–392.

[19] L. Huang, S. Wu, X. Li, Reduced-rank MDL method for source enumeration in high-resolution array processing, IEEE Trans. Signal Process. 55 (December (12)) (2007) 5658–5667.

[20] L. Huang, T. Long, S. Wu, Source enumeration for high-resolution array processing using improved Gerschgorin radii without eigen-decomposition, IEEE Trans. Signal Process. 56 (December (12)) (2008) 5916–5925.

[21] M. Abramowitz, I. Stegun (Eds.), Handbook of Mathematical Functions, Dover, New York, 1970.

[22] M.A. Doron, E. Doron, Wavefield modeling and array processing. Part I. Spatial sampling, IEEE Trans. Signal Process. 42 (October (10)) (1994) 2549–2559.

[23] L. De Lathauwer, J. Castaing, Blind identification of underdetermined mixtures by simultaneous matrix diagonalization, IEEE Trans. Signal Process. 56 (March (3)) (2008) 1096–1105.